Universiteit
Leiden
The Netherlands

Dynamics of the Oort cloud and formation of interstellar comets

Torres Rodriguez, S.

Citation
Torres Rodriguez, S. (2020, April 30). *Dynamics of the Oort cloud and formation of interstellar comets*. Retrieved from https://hdl.handle.net/1887/87515

Version:	Publisher's Version
License:	Licence agreement concerning inclusion of doctoral thesis in the Institutional Repository of the University of Leiden
Downloaded from:	https://hdl.handle.net/1887/87515

Note: To cite this publication please use the final published version (if applicable).

Cover Page

Universiteit Leiden

The handle http://hdl.handle.net/1887/87515 holds various files of this Leiden University dissertation.

Author: Torres Rodriguez, S.
Title: Dynamics of the Oort cloud and formation of interstellar comets
Issue Date: 2020-04-30

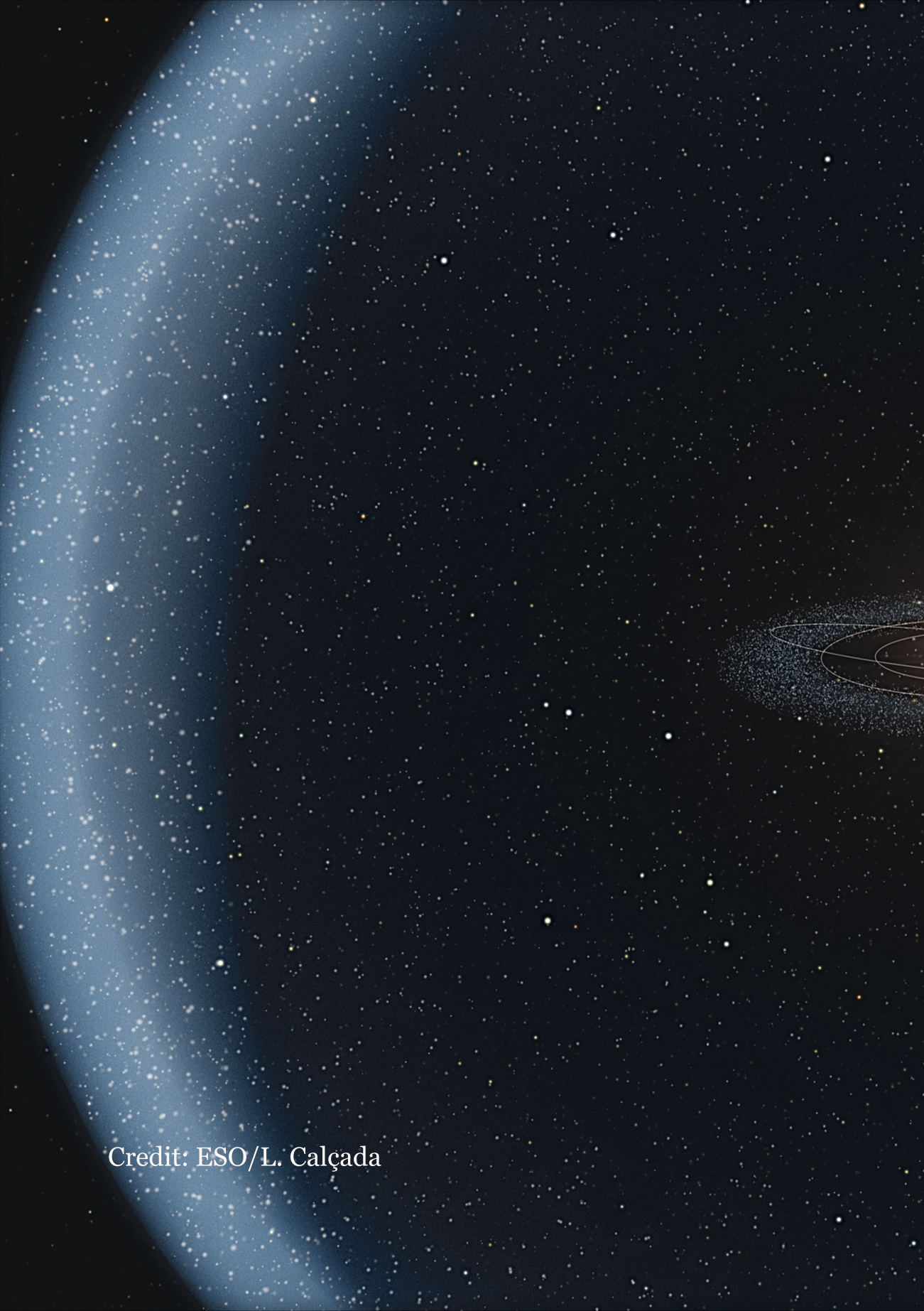

Credit: ESO/L. Calçada

Chapter 3

Galactic tide and local stellar perturbations on the Oort cloud: creation of interstellar comets

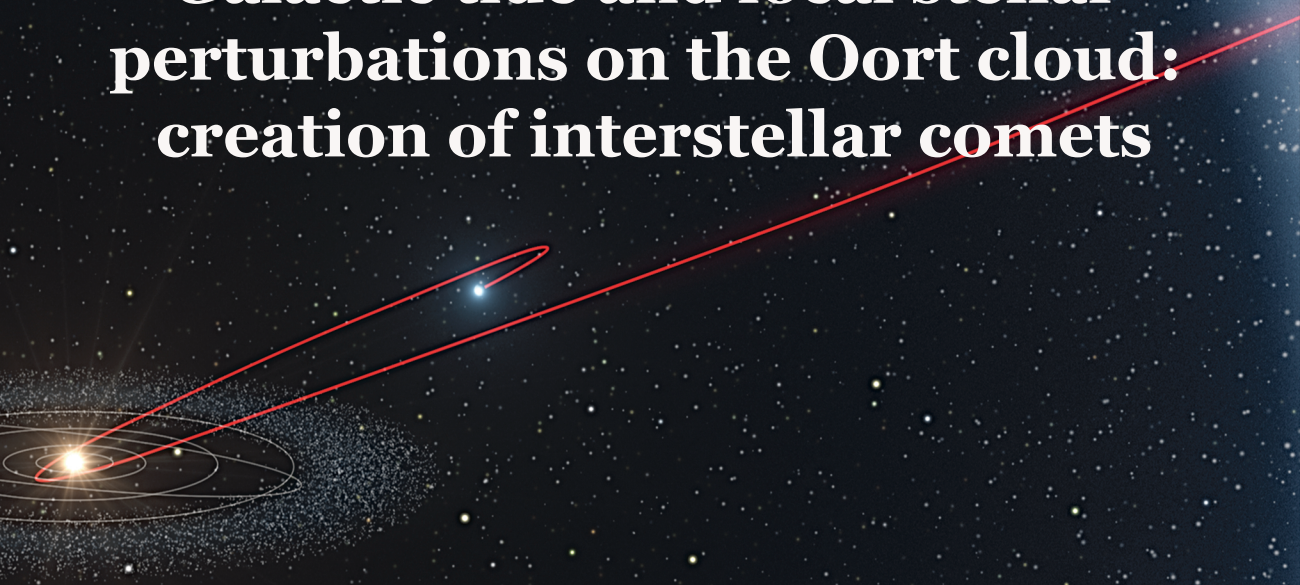

S. Torres, M. X. Cai,
S. Portegies Zwart, and A. G. A. Brown
Astronomy & Astrophysics
629, A139 2019a

Abstract

Comets in the Oort cloud evolve under the influence of internal and external perturbations, such as giant planets, stellar passages, and the Galactic gravitational tidal field. We aim to study the dynamical evolution of the comets in the Oort cloud, accounting for the perturbation of the Galactic tidal field and passing stars. We base our study on three main approaches; analytic, observational, and numerical. We first construct an analytical model of stellar encounters. We find that individual perturbations do not modify the dynamics of the comets in the cloud unless very close ($<$ 0.5 pc) encounters occur. Using proper motions, parallaxes, and radial velocities from *Gaia* DR2 and combining them with the radial velocities from other surveys, we then construct an astrometric catalogue of the $14\,659$ stars that are within 50 pc of the Sun. For all these stars we calculate the time and distance of closest approach to the Sun. We find that the cumulative effect of relatively distant ($\leqslant 1$ pc) passing stars can perturb the comets in the Oort cloud. Finally, we study the dynamical evolution of the comets in the Oort cloud under the influence of multiple stellar encounters from stars that pass within 2.5 pc of the Sun and the Galactic tidal field over ± 10 Myr. We use the Astrophysical Multipurpose Software Environment (AMUSE), and the GPU-accelerated direct N-body code ABIE. We considered two models for the Oort cloud, compact ($a \leqslant 0.25$ pc) and extended ($a \leqslant 0.5$ pc). We find that the cumulative effect of stellar encounters is the major perturber of the Oort cloud for a compact configuration while for the extended configuration the Galactic tidal field is the major perturber. In both cases the cumulative effect of distant stellar encounters together with the Galactic tidal field raises the semi-major axis of $\sim 1.1\%$ of the comets at the edge of the Oort cloud up to interstellar regions ($a > 0.5$ pc) over the 20 Myr period considered. This leads to the creation of transitional interstellar comets (TICs), which might become interstellar objects due to external perturbations. This raises the question of the formation, evolution, and current status of the Oort cloud as well as the existence of a "cloud" of objects in the interstellar space that might overlap with our Oort cloud, when considering that other planetary systems should undergo similar processes leading to the ejection of comets.

Section 3.1

Introduction

The outer region of the solar system is populated by a large number of planetesimals. Further away, more than $1\,000$ au from the Sun, and almost extending to the nearest stars, is the Oort cloud. Its existence was proposed in the late 1950s by the Dutch astronomer Jan Hendrik Oort, who realised that long-term comets (with orbital semi-major axes $a > 40$ au) bound to the Sun must come from an area well beyond Neptune. Oort (1950) pointed out that a spike in the distribution of $1/a$ of the long-period comets with $a > 10^4$ au, and isotropic inclinations in $\cos i$, ω, and Ω, would argue for the existence of a reservoir of objects in quasi-spherical symmetry surrounding the solar system. The Oort cloud has remained unobserved to date.

There have been numerous studies aimed at trying to explain the formation, evolution, and structure of the Oort cloud, mostly through numerical simulation (e.g. Hills 1981; Heisler & Tremaine 1986; Duncan et al. 1987; Weissman 1996; Wiegert & Tremaine 1999; García-Sánchez et al. 1999; Dybczyński 2002; Levison et al. 2004; Dones et al. 2004; Morbidelli 2005; Duncan 2008; Brasser et al. 2006; Fouchard et al. 2006; Kaib & Quinn 2008; Brasser & Morbidelli 2013; Shannon et al. 2014; Dones et al. 2015). There is general agreement on some properties of the Oort cloud, in particular that it is composed of the residual planetesimals after the planet formation epoch. The Oort cloud is divided into two regions: the *inner* Oort cloud is usually reserved for comets with semi-major axes $a < 20\,000$ au and is invisible unless there is a comet shower. The *outer* Oort cloud refers to comets with semi-major axes $a > 20\,000$ au (e.g. Dones et al. 2015). Its shape is thought to be nearly spherical and limited at 0.5 pc mainly by the influence of the Galactic tidal field and stellar flybys (e.g. Heisler & Tremaine 1986). The Oort cloud is thought to contain around 10^{12} objects with a total mass of $\sim 3 \times 10^{25}$ kg (e.g. Morbidelli 2005). However, these estimations are highly uncertain. The above-mentioned studies also concluded that in order for long-period comets to still exist today they need to be replenished. Otherwise they would have been depleted on a timescale much shorter than the lifetime of the solar system.

The orbits of the comets in the Oort cloud form a frozen record of the evolution of the solar system and preserve the memory of its birth environment (Portegies Zwart & Jílková 2015; Martínez-Barbosa et al. 2016; Fouchard et al. 2011, 2018). External perturbations such as Galactic tides,

stellar flybys, and molecular clouds play an important role in the understanding of the formation and evolution of the Oort cloud and Oort cloud-like structures in other planetary systems (see e.g. Veras et al. 2013, 2014). Passing stars can perturb the comets, changing their perihelion distances much more than they change the overall size of the orbit, changing the cometary trajectories and injecting the comets into the inner solar system (Morbidelli 2005 and Duncan 2008). The outer Oort cloud has been affected quite substantially by external influences. Not only by passing stars in the parental cluster of the Sun but also by occasional relatively close encounters that have occurred after the Sun has left its birth cluster (Jílková et al. 2016). Jílková et al. (2015) pointed out that the planetesimals *Sedna* and *2008PV113* belong to the inner Oort cloud and that they may have been captured during an encounter with another star in the birth cluster of the Sun. This star is conjectured to have passed the solar system within about 340 au and would have deposited approximately $1\,400$ other planetesimals together with the two currently known objects in this family. The orbital characteristics of these objects share similar properties which can be used to reconstruct the encounter.

Close encounters with the solar system have been studied by a number of authors (e.g. Rickman 1976; Robert A. J. Matthews 1994; Weissman 1996; Dehnen & Binney 1998; García-Sánchez et al. 1999; Levison et al. 2004; Jimenez-Torres et al. 2011; Bailer-Jones 2015; Dybczyński & Berski 2015; Higuchi & Kokubo 2015; Feng & Bailer-Jones 2015; Berski & Dybczyński 2016). Most of them calculated the closest encounters with the solar system within ± 10 Myr using the astrometric data of the stars in the solar neighbourhood (< 50 pc) provided by Hipparcos mission (Perryman et al. 1997). They find that the closest approach (~ 0.3 pc) in the future (~ 1.3 Myr from the present) will be with the star HIP 8982 (GJ 710), which will cause minor changes in the perihelion distance of the comets. The most recent close stellar encounter was with the so-called Scholz's star ($M_\star \simeq 0.15$ M$_\odot$ at a distance of $0.25^{+0.11}_{-0.07}$ pc, Scholz 2014, Mamajek et al. 2015). All of the studies cited above were limited by the observational data due to the incompleteness of the Hipparcos survey.

The first data release (*Gaia* DR1) of the European Space Agency's *Gaia* mission (Gaia Collaboration, Brown et al. 2016; Gaia Collaboration et al. 2016) opened a new window for understanding the Milky Way. In the particular case of the solar system, *Gaia* detected nearly all of the local star systems within 50 pc of the Sun (compared to the 20% detected by Hipparcos). Using *Gaia* DR1, several authors (Berski & Dybczyński 2016; Bobylev

& Bajkova 2017; Torres et al. 2018; Bailer-Jones 2018) re-computed the orbit of the closest stars to the Sun. They found new stars and new parameters for some of the very well known encounters, such as GJ 710, which gets closer (0.064 pc) based on the *Gaia* DR1 data. The recent second *Gaia* data release – *Gaia* DR2 (Gaia Collaboration et al. 2018) –, provided 7.2 million radial velocities. This provided an opportunity to find new and more accurately characterised stellar encounters. Using *Gaia* DR2, Bailer-Jones et al. (2018) found 693 new stars with closest-encounter distances within 5 pc and 15 Myrs from now; accounting for the incompleteness they also re-calculate the present rate of encounters, which within ~ 1 pc of the Sun is estimated to be 20 ± 2 Myr^{-1}. From Hipparcos data García-Sánchez et al. (1999) derived 11.7 ± 1.3 Myr^{-1} within ~ 1 pc and Martínez-Barbosa et al. (2017) employed simulations to derive rates of 21, 39, and 63 Myr^{-1} within ~ 2 pc for three different scenarios (orbital migration from the Milky Way inner disk, migration from the outer disk, and no migration, respectively).

We aim to obtain a conservative estimate of the combined effects of stellar encounters and the Galactic tidal field on the Oort cloud, by only considering the encounters from stars listed in *Gaia* DR2 within ± 10 Myr from the present. The latter sample is incomplete and thus provides a lower limit on the effects of passing stars. In Sect. 5.2 we present a simple analytical model for stellar encounters and discuss the cumulative effect of passing stars on the Oort cloud, using the impulse approximation. In Sect. 5.3 we present a catalogue of nearby stars and we calculate the effect of individuals encounters with stars within 2.5 pc of the Sun. In Sect. 5.4 we present a numerical model for multiple stellar encounters and study the dynamical evolution of a simulated Oort cloud after the interaction with the nearby stars and the Galactic tidal field. Finally, in Sect. 3.5 we present our summary and conclusions.

Section 3.2

Model for stellar encounters

The estimated extent of the Oort cloud is $\sim$ 0.5pc (Oort 1950; Dones et al. 2015), which means that the orbital velocity of bodies in the Oort cloud is limited to 0.13 km s^{-1}. This implies that comets at the edge of the Oort cloud are barely bound to the Sun and thus the condition for a comet ejection due to an external perturbation, $\Delta v_{\perp} > v_{\rm esc}$ (where $v_{\rm esc}$ is the escape velocity) is easily met. The Galactic tidal field is the most important perturbation to the outer Oort cloud at large distances (Heisler & Tremaine 1986). However close encounters with stars also play an important role in the evolution of the Oort cloud.

3.2.1 Analytic model

A simple analytical model of stellar encounters can help us to better understand the effect of passing stars on the Oort cloud. To construct such a model, we followed the works of Rickman (1976); García-Sánchez et al. (2001); Rickman et al. (2004, 2008); Martínez-Barbosa et al. (2017). We first compiled data for the mass, velocity dispersion, and the space density of the stars in the solar neighbourhood for 13 spectral types, as in Table 8 in García-Sánchez et al. (2001). The mass of the stars corresponding to the spectral types B0V to M5V was taken from the data compiled by Mamajek (2018)[*] (see also Pecaut & Mamajek 2013). While the mean value for white dwarfs (WD) was taken from Jiménez-Esteban et al. (2018). The peculiar velocity of the Sun ($v_{\odot}$) and the velocity dispersion of the stars (v_{*}) were taken from Rickman et al. (2008). The space density of spectral types A to K and Giants was obtained from Bovy (2017). For B and M type stars the values were obtained from Rickman et al. (2008), and for the WD from Jiménez-Esteban et al. (2018). The compiled data are shown in Table 3.1.

We consider the effect of the stars with different masses (M_{*}) and spectral types in the solar neighbourhood on the comets in the Oort cloud. We assume that the stars move on a straight line trajectory, and with a constant velocity relative to the Sun (v_{*}). For high stellar velocities, we can assume that the comet is at rest during the stellar passage. Using the impulse approximation (Oort 1950; Rickman 1976), we then calculate the change of the velocity ($\Delta V_{\perp}$) imparted to a comet in the Oort cloud due to a random

[*] http://www.pas.rochester.edu/~emamajek/EEM_dwarf_UBVIJHK_colors_Teff.txt

Table 3.1: Stellar parameters. Columns represent the spectral type of the stars followed by their mass, velocity dispersion, and the peculiar velocity of the Sun with respect to each spectral type. The relative velocity of the encounter within the Sun–comet system and the star is shown in column 5. The number density of stars in the solar neighbourhood is shown in column 6.

$S.T$	$M_*[M_\odot]$	$v_*[\mathrm{km\ s^{-1}}]$	$v_\odot[\mathrm{km\ s^{-1}}]$	$v_{enc}[\mathrm{km\ s^{-1}}]$	$\rho_*[10^{-3}pc^{-3}]$
BoV	15	14.7	18.6	24.6	0.06
AoV	2.3	19.7	17.1	27.5	0.26
A5V	1.85	23.7	13.7	29.3	0.34
FoV	1.59	29.1	17.1	36.5	0.61
F5V	1.33	36.2	17.1	43.6	1.51
GoV	1.08	37.4	26.4	49.8	1.61
G5V	0.98	39.2	23.9	49.6	1.73
KoV	0.87	34.1	19.8	42.6	4.21
K5V	0.68	43.4	25.0	54.3	5.26
MoV	0.55	42.7	17.3	50.0	8.72
M5V	0.16	41.8	23.3	51.8	41.55
WD	0.6	63.4	38.3	80.2	4.9
Giants	2.2	41.0	21.0	49.7	3.9

stellar encounter by integrating the perpendicular force generated by each passing star:

$$\Delta V_\perp \approx \frac{2GM_*}{v_*}\left[\frac{\mathbf{r_c}}{r_c^2} - \frac{\mathbf{r}_\odot}{r_\odot^2}\right], \tag{3.1}$$

where r_c and $r_\odot$ correspond to the vectors from the comet and the Sun to the point of closest approach of the star (assuming that the comet has not been deflected by the gravity of the star). If we consider r the heliocentric distance of the comet and we assume that the distance of the encounter is large enough compared to the distance Sun–comet, we can approximate Equation (3.1) with:

$$\Delta V_\perp \propto \frac{M_* r}{v_* r_\odot^2}. \tag{3.2}$$

For the case of a very close encounter with the comet, Equation (5.3) can be approximated as

$$\Delta V_\perp \propto \frac{M_*}{v_* r_c}. \tag{3.3}$$

It is important to stress that the impulse approximation is based on a number of simplifying assumptions, and therefore it should be used for statistical analysis only. For our propose, it gives us a general idea of the effect of the different stars in the solar neighbourhood on the comets in the Oort cloud.

Following Rickman (1976) we can calculate the frequency of the stellar encounters using

$$f = \pi r_*^2 v_{\rm enc} \rho_* \,, \tag{3.4}$$

where r_* is the distance of the encounter, $v_{\rm enc}$=$\sqrt{v_\odot^2 + v_*^2}$ is the relative velocity of the Sun and a random passing star ($v_\odot$ represents the peculiar velocity of the Sun, and v_* the velocity dispersion of the parent population of the passing star), and ρ_* is the number density of stars of a given spectral type in the solar neighbourhood. Equation (3.4) can be used to determine the number of stars passing by within a sphere of radius $r_{\rm s}$ centred on the Sun or a random comet (assuming that stars of the solar neighbourhood are uniformly distributed at any time and the stellar velocities relative to the Sun are constant, Rickman 1976):

$$N_* = r_{\rm s}^2 f t \,. \tag{3.5}$$

3.2.2 Perturbations on the Oort cloud

Using Eq. (5.3) and the values in Table 3.1, we calculated the frequency of the stars passing within a distance r_* from the Oort cloud. We find that the total frequency of stars passing within 1 pc is around 12.5 Myr^{-1} (see Table 3.2). Following the same method, García-Sánchez et al. (1999) found a lower value (11.7 Myr^{-1}). The main difference with our result is due to the updated values for the mass and density of the stars used in this work. The most probable perturber of the Oort cloud is the low mass, high-relative-velocity stars.

Using Eq. (5.3), in Fig. 3.1 we show the change of the velocity of a comet due to an encounter with a star for different spectral types and as a function of the distance of the encounter for an interval of 0.1–2.5 pc. The lower distance corresponds to the inner Oort cloud, while the larger distance corresponds to the limit where a passing star can start perturbing a comet at

Table 3.2: Analytical model for stellar encounters for an encounter distance of 1 pc. The spectral type is shown in column 1, the frequency of the stellar encounters is shown in column 2, the change in the velocity of a comet due to an interaction with a star is shown in column 3, and the total number of stars entering a sphere of radius 1 pc around the Sun–comet system over a time interval of 1 *Gyr* is shown in column 4.

S.T	$f_*^{1\mathrm{pc}}$ [Myr^{-1}]	$\Delta V_{\perp,*}^{1\mathrm{pc}}$ [km s^{-1}]	$N_*^{1\mathrm{pc}}$
B0V	0.005	8.77e-03	4.742
A0V	0.023	1.005e-03	22.973
A5V	0.032	6.716e-04	32.007
F0V	0.072	4.701e-04	71.536
F5V	0.212	3.161e-04	211.527
G0V	0.258	2.485e-04	257.608
G5V	0.276	2.151e-04	275.696
K0V	0.576	2.195e-04	576.229
K5V	0.918	1.348e-04	917.675
M0V	1.401	1.108e-04	1400.844
M5V	6.915	3.293e-05	6915.189
WD	1.263	8.143e-05	1262.623
Giants	0.623	4.617e-04	622.765

the edge of the cloud. In the rest of this work we refer to the latter distance as the *critical radius*.

As shown in Fig. 3.1 the change induced by a single encounter is relatively small. Massive stars are effective in exciting the object in the Oort cloud, but they are rare. Low-mass stars are very common, but their effect on the orbits of a comet is small. However the number of stars encountering the solar system increases over time.

The model presented in this section is based on a number of simplifying assumptions. Specifically, the impulse approximation provides a quick but inaccurate estimate of the effect of a random passing star on a comet in the Oort cloud. As we show in Table 3.2 the effect of individual stars is relative small. However, considering the frequency and the number of stars approaching the Sun to within 1 pc over 1 Gyr, their cumulative effect might change the structure and dynamics of the Oort cloud. In order to have a better understanding of the evolution of the Oort cloud it is necessary to employ a detailed numerical model which accounts for the effects of the Galactic tidal field and stellar distribution of stars around the

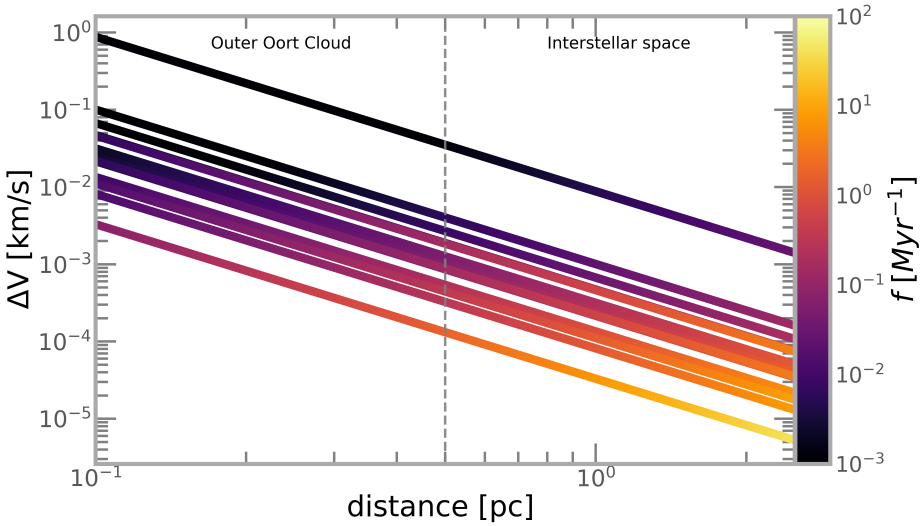

Figure 3.1: Change of the velocity of a comet due to random stellar encounters for the 13 stellar spectral types listed in Table 3.1 as a function of the encounter distance. The colour coding of the lines represents the frequency of stellar encounters as a function of the distance of the encounter for the corresponding types of stars. The lines represent the different spectral types in the order listed in Table 3.1. The mass of the stars decreases from the top to the bottom lines.

Sun. In Sect. 5.3 we present a list of nearby stars within 50 pc of the Sun for which *Gaia* DR2 astrometry and radial velocities (including from other surveys) are available. This provides us with accurate kinematic information on nearby stars that could influence the Oort cloud in the recent past or near future. In Sect. 5.4 we use numerical simulations to analyse their effect on the comets in the Oort cloud and estimate their cumulative effect over ± 10 Myr, including the effect of the Galactic tidal field.

Section 3.3

Close encounters with the solar system

Our knowledge of close stellar encounters in the recent past or near future has been limited by the availability of precise and accurate astrometry and radial velocities for the nearby stars. The Gaia mission has considerably increased the availability of astrometric and radial velocity data for the

closest stars, even if about 20% of the stars with high proper motions are not listed in *Gaia* DR2 and those tend to be close to the Sun (Bailer-Jones et al. 2018).

Table 3.3: Overview of the catalogue of stars within 50 pc of the Sun for which encounter parameters were calculated. The full catalogue can be download from: https://home.strw.leidenuniv.nl/~storres/#Research

Input catalogue(s)	No. Stars $\leqslant 50$ pc
Gaia DR2	10,744
Gaia DR2 + RAVE DR5	2356
Gaia DR2 + GALAH DR2	11
Gaia DR2 + LAMOST DR3	307
Gaia DR2 + APOGEE DR14	1092
Gaia DR2 + XHIP	149
Total	14 659

3.3.1 Observational model

To construct the list of stars within 50 pc of the Sun for which the encounter parameters (closest approach distance, velocity, and time) can be calculated we used the data from the *Gaia* DR2 catalogue. To increase the number of stars for which radial velocity information is available we cross-matched *Gaia* DR2 with the following catalogues: RAVE-DR5 (Kunder et al. 2017), GALAH DR2 (Buder et al. 2018), LAMOST DR3 (Zhao et al. 2012), APOGEE DR14 (Abolfathi et al. 2018), and XHIP (Anderson & Francis 2012). We selected only stars with relative uncertainty on the parallax (ϖ) smaller than 20%, such that $1/\varpi$ is a good estimator of the distance to the stars. Following Lindegren et al. (2018) we further filtered the list of stars according to

$$u^2 < 1.44 \times \max[1, \exp(-0.4(G - 19.5))], \tag{3.6}$$

and

$$1.0 + 0.015(G_{\rm BP} - G_{\rm RP})^2 < E < 1.3 + 0.06(G_{\rm BP} - G_{\rm RP})^2\,, \tag{3.7}$$

where G, $G_{\rm BP}$, and $G_{\rm RP}$ correspond to the photometric measurements, covering a wavelength from the near-ultraviolet to the near-infrared for the

G passband, 330 to 680nm, and 630 to 1050 nm for $G_{\rm BP}$, and $G_{\rm RP}$, respectively. The $u = (\chi^2/\nu)^{1/2}$ corresponds to the unit weight error, and E is the flux excess factor. This filter selects sources with high-quality astrometry and weeds out stars which appear to be nearby because of spuriously high values of the parallax (see appendix C in Lindegren et al. 2018). The resulting catalogue contains $14\,659$ stars within 50 pc of the Sun (Table 3.3).

For the selected stars we estimated the distance, time, and velocity of closest approach using the linear approximation method of Robert A. J. Matthews (1994) in the formulation presented in Bailer-Jones (2015):

$$v_{\rm tot} = \sqrt{v_{\rm T}^2 + v_{\rm rad}^2} \tag{3.8}$$

$$t_{\rm ph} = -\frac{c v_{\rm rad}}{\varpi v_{\rm tot}^2} \tag{3.9}$$

$$d_{\rm ph} = \frac{10^3}{\varpi}\frac{v_{\rm T}}{v_{\rm tot}}\,, \tag{3.10}$$

where $v_{\rm T} = 4.74\left[({\mu_{\alpha*}}^2 + {\mu_\delta}^2)^{0.5}/\varpi\right]$ is the transverse velocity, $v_{\rm rad}$ is the radial velocity of the star, ϖ is the parallax, $c = 10^3$ pc km^{-1} yr^{-1}, and the subscript 'ph' stands for perihelion. We estimated the mass of the stars using the effective temperature provided in *Gaia* DR2 (Andrae et al. 2018) and linearly interpolating in the Tables in Mamajek (2018) and Pecaut & Mamajek (2013).

Of the $14\,659$ stars within 50 pc there are 31 that pass within 2.5 pc of the Sun (Fig. 3.2, big dots) over a period of 20 Myr centred on the present (i.e. 10 Myr in the past and 10 Myr in the future). Figure 3.2 shows the observational Hertzsprung-Russell diagram of our sample. In Fig. 3.3 we show the closest approach distance and time of the stars in our sample with respect to the Sun. The limited distance range of the stars under study only allows us to find very close encounters within ± 3 Myr.

In Fig. 3.3 the large dots show the distribution of the stars passing within 2.5 pc and those tend to be the major perturber of the Oort cloud (referred to as '*Gaia* stars' below). The closest encounter with the solar system is GJ 710 which will penetrate deep inside the inner Oort cloud. As shown in Fig. 3.2 most of the closest encounters involve M dwarfs, with a considerable fraction of solar type stars. This implies that the effect of a single encounter with the Oort cloud will be minimal, mainly due to the low mass of the perturber and its high velocity with respect to the Sun.

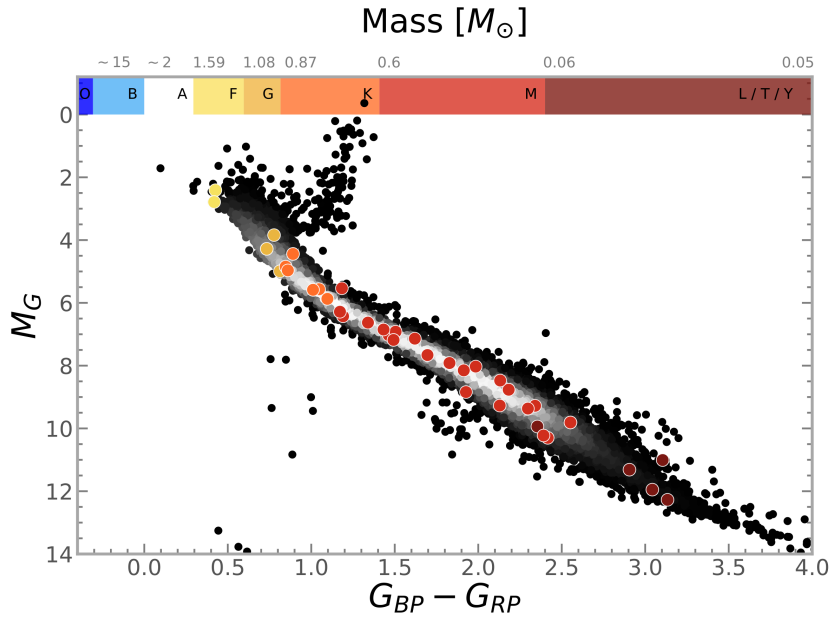

Figure 3.2: Observational HR diagram of the nearby stars contained in the catalogue summarised in Table 3.3. The big dots represent the stars within 2.5 pc of the Sun colour coded according to their spectral type. The density map shows all the stars in our sample.

Bailer-Jones et al. (2018) find 62 new stellar encounters, which partially overlap with our list. Their list of encounters is larger than ours mostly because they did not apply the strict filtering on the astrometric quality of the *Gaia* DR2 data employed in this work. For stars appearing in both studies we find similar results.

We stress that the sample of the closest stars presented here is incomplete. The observational incompleteness is evident in the decrease in encounter frequency as one moves away from the present epoch in time. A complete census of stellar encounters requires all the stars within a certain distance to be identified. The main limitations in using the *Gaia* survey for finding the closest encounters are the survey magnitude limit, which prevents the identification of encounters with faint low-mass stars, and the lack of radial velocities. The *Gaia* DR2 radial velocity survey is limited to effective temperatures in the range $\sim$ 3550–6900 K and to stars brighter than $G = 14$ mag (see e.g. Bailer-Jones et al. 2018). An additional lim-

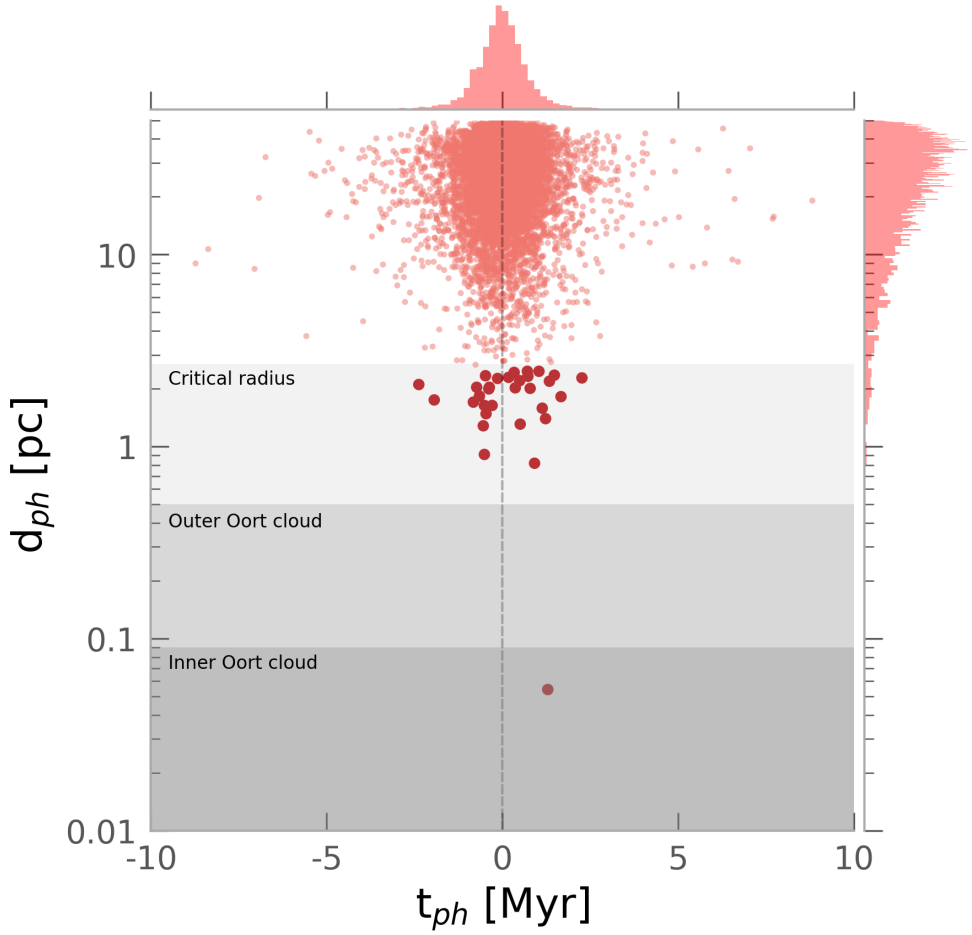

Figure 3.3: Closest approach distance vs. closest approach time. The shaded areas represent the critical radius within which stars can affect an object in the Oort cloud, and the boundaries of the outer and inner Oort cloud, respectively. The big dots correspond to those stars that pass within 2.5 pc of the Sun.

itation is that some of the brightest stars in the sky are missing from the *Gaia* DR2 catalogue (Gaia Collaboration et al. 2018).

A detailed study correcting for incompleteness in *Gaia* DR2 was carried out by Bailer-Jones et al. (2018). These latter authors constructed a completeness map (Fig. 12, Bailer-Jones et al. 2018), interpreted as the probability of detecting a given close encounter in the *Gaia* DR2 sample. They found that only 15% of the encounters within 5 pc in a period of 5 Myr have been identified. Using this result, the authors used a simulated Milky Way galaxy to infer the encounter rate averaged over 5 Myr, in the past and future. They found that the encounter rate of stellar encounters within 1 pc is 20 ± 2 Myr^{-1}.

3.3.2 Stellar encounters with the Solar System

In Section 3.3.1 we employed a simple method to estimate the perihelion distances and times for stars approaching the Sun by assuming the stars follow a uniform motion along straight lines with respect to the Sun (see also Bailer-Jones 2015). We now seek a better estimation of the perihelion distance through the joint integration of the orbits of the Sun and the stars that are predicted to approach to within 2.5 pc (Table 3.4) backwards and forwards in time for 10 Myr. We first transformed the astrometric and radial velocity data into galactocentric Cartesian frame using `Astropy` (The Astropy Collaboration et al. 2018). We adopted the position of the Sun and the local circular velocity parameters from Reid et al. (2014): $Z_\odot = 27$ pc, $R_\odot = 8.34$ kpc, and $V_{c,\odot} = 240$ km s^{-1}; while the peculiar velocity of the Sun was adopted from Schönrich et al. (2010): $(U_\odot, V_\odot, W_\odot) = (11.1, 12.24, 7.25)$ km s^{-1}. We used the `Gala` (Price-Whelan 2017) package to perform the orbital integration. The Milky Way potential used is described by an analytic axisymmetric model which contains a spherical nucleus and bulge (Hernquist 1990), a Miyamoto-Nagai disk (Miyamoto & Nagai 1975; Bovy 2015), and a spherical Navarro-Frenk-White (NFW) dark matter halo (Navarro et al. 1996).

To account for the observational uncertainties we sample the astrometric and radial velocity observables for each star, taking the full covariance matrix into account. For each star, 10^6 samples of the astrometry and radial velocity are drawn and for each of these the above described orbit integration is carried out. The end result is a sampling of the distribution of possible perihelion distances and times. This distribution obtained through Monte Carlo sampling is then treated as the probability density function

(PDF) of the encounter parameters. The shape of the confidence regions is mainly affected by the relative errors on parallax and radial velocity. The relative error in the proper motion likewise affects the shape of the confidence regions around the mean. Figures 3.4, 3.5, and 3.6 show the resulting PDFs.

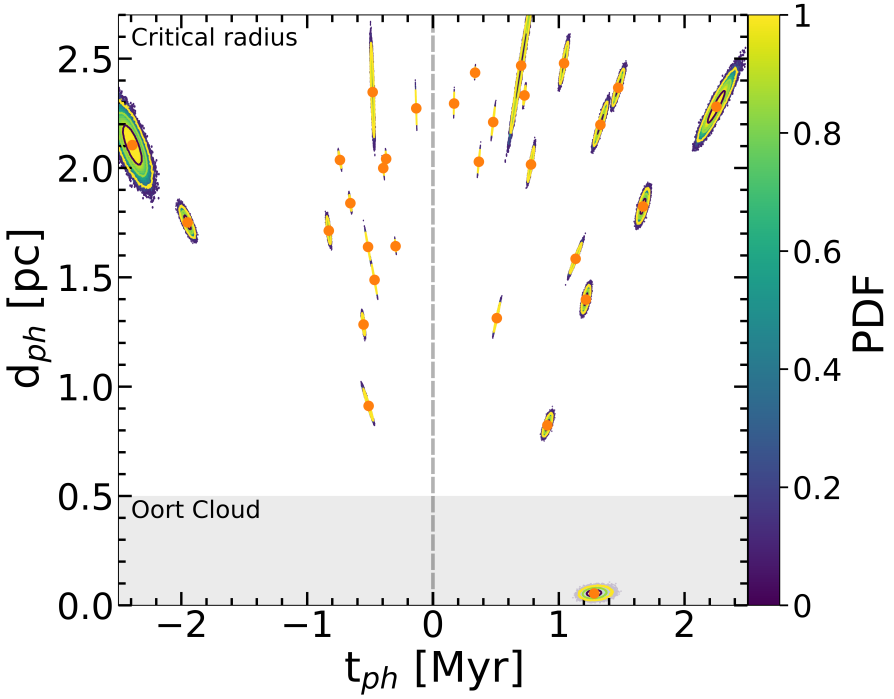

Figure 3.4: Joint probability density of the time and distance of closest approach for those stars that are predicted to pass within 2.5 pc of the Sun (listed in Table 3.3). The contour levels indicate regions enclosing 0.6, 0.9, and 0.99 % cumulative probability (colour bar). The shape of each PDF is affected by the relative errors in the observational data of each star, particularly the errors on parallax and radial velocity.

In Fig. 3.4 we show the distribution of time and distance of closest approach for the time interval ± 3 Myr from the present.The closest encounter found is, as expected, the very well known case of GJ 710.In Fig. 3.5 we show the distribution of the total relative velocity and distance of closest approach. Most stars in our sample have high velocities (20 to 80 km s^{-1}) meaning that their effect on the Oort cloud is small. Figure 3.6 shows the

Table 3.4: Stars predicted to approach the Sun within 2.5 pc over the ±10 Myr from today. The columns represent the Gaia DR2 ID, the time, distance and velocity at the perihelion with its respective confidence interval. These are followed by the effective temperature listed in Gaia DR2, the estimated mass of the star, and the change in the velocity due to the encounter with the Sun for each star.

Gaia DR2 ID	$t_{\rm ph}$ [Myr]	$t_{\rm sample}$	$d_{\rm ph}$[pc]	$d_{\rm sample}$	$v_{\rm tot}$ [km s^{-1}]	$v_{\rm sample}$	$T_{\rm eff}$ [K]	Mass [M$_\odot$]	$\Delta v_\perp$ [km s^{-1}]
4270814637616488064	1.282	[1.123 , 1.488]	0.054	[0.006 , 0.107]	14.525	[12.515 , 16.564]	4116	0.654	1.305e-01
553219967007245312	1.670	[1.595 , 1.742]	1.824	[1.714 , 1.952]	24.163	[23.187 , 25.284]	5175	0.851	9.106e-05
258179971749627776	0.365	[0.352 , 0.378]	2.028	[1.955 , 2.107]	78.377	[75.746 , 81.470]	4507	0.717	1.915e-05
4575928186606190336	0.479	[0.462 , 0.500]	2.210	[2.126 , 2.307]	51.102	[48.983 , 52.973]	3795	0.559	1.925e-05
3240424426786618624	−0.552	[−0.572 , −0.534]	1.284	[1.214 , 1.368]	83.029	[80.325 , 85.666]	3836	0.580	3.647e-05
4795598309045006208	−0.739	[−0.757 , −0.723]	2.037	[1.985 , 2.091]	32.470	[31.698 , 33.194]	5343	0.901	5.755e-05
3274130814728561792	−2.390	[−2.645 , −2.158]	2.105	[1.834 , 2.447]	19.171	[17.362 , 21.165]	4471	0.715	7.240e-05
981375326780564608	0.508	[0.476 , 0.548]	1.314	[1.229 , 1.422]	53.595	[49.613 , 57.211]	3875	0.601	5.589e-05
6684504722300935680	−0.465	[−0.495 , −0.436]	1.488	[1.400 , 1.587]	43.104	[40.449 , 45.973]	3619	0.494	4.451e-05
4430238051199001216	0.167	[0.165 , 0.171]	2.295	[2.225 , 2.379]	67.699	[66.901 , 68.396]	6017	1.128	2.724e-05
2417069815934357248	2.253	[2.049 , 2.486]	2.280	[2.068 , 2.531]	14.047	[12.746 , 15.408]	4613	0.741	8.735e-05
3089711447388931584	−0.133	[−0.139 , −0.127]	2.273	[2.164 , 2.389]	63.544	[60.457 , 66.818]	3820	0.571	1.497e-05
3339921875389105152	−0.516	[−0.544 , −0.485]	1.639	[1.541 , 1.732]	21.455	[20.317 , 22.843]	4105	0.653	9.746e-05
1134618591670426112	0.728	[0.713 , 0.742]	2.331	[2.273 , 2.394]	63.885	[62.639 , 65.223]	4887	0.787	1.950e-05
5861048509766415616	−0.297	[−0.304 , −0.290]	1.643	[1.601 , 1.682]	59.275	[57.962 , 60.702]	3795	0.559	3.005e-05
681999884156922368	1.134	[1.066 , 1.209]	1.585	[1.483 , 1.697]	15.785	[14.795 , 16.794]	3956	0.615	1.336e-04
3260079227925564160	0.910	[0.851 , 0.968]	0.823	[0.754 , 0.905]	33.395	[31.465 , 35.704]	3998	0.629	2.395e-04
2648914040357320576	1.473	[1.412 , 1.544]	2.367	[2.257 , 2.502]	13.235	[12.616 , 13.823]	5630	0.976	1.133e-04
3972130276695660288	−0.511	[−0.572 , −0.458]	0.912	[0.818 , 1.025]	31.845	[28.459 , 35.551]	3980	0.623	2.025e-04
2118161219075485824	0.779	[0.743 , 0.816]	2.016	[1.908 , 2.126]	56.180	[53.650 , 58.906]	4122	0.654	2.466e-05
1392610405193517952	0.702	[0.586 , 0.882]	2.468	[2.067 , 3.095]	64.956	[51.343 , 77.613]	5057	0.823	1.790e-05
2089889682751105536	1.041	[0.997 , 1.090]	2.478	[2.346 , 2.633]	46.407	[44.351 , 48.454]	3965	0.618	1.866e-05
2272191085754928768	0.335	[0.331 , 0.338]	2.436	[2.401 , 2.469]	76.760	[75.892 , 77.614]	5859	1.060	2.003e-05
4758877919212831104	−0.395	[−0.405 , −0.385]	2.000	[1.952 , 2.050]	31.680	[30.850 , 32.497]	4893	0.788	5.352e-05
4839132097557586560	−0.828	[−0.856 , −0.803]	1.713	[1.624 , 1.815]	46.116	[44.687 , 47.522]	3865	0.597	3.798e-05
5076269164798852864	−0.479	[−0.503 , −0.456]	2.347	[2.063 , 2.673]	50.434	[49.277 , 51.577]	4837	0.781	2.418e-05
4546557031272743680	1.216	[1.163 , 1.272]	1.398	[1.311 , 1.490]	35.688	[34.137 , 37.245]	4305	0.695	8.573e-05
875071278432954240	1.331	[1.250 , 1.413]	2.198	[2.057 , 2.351]	16.389	[15.429 , 17.455]	5714	0.998	1.085e-04
2924339469735490560	−1.951	[−2.039 , −1.862]	1.751	[1.646 , 1.864]	14.766	[14.128 , 15.488]	5743	1.009	1.918e-04
3371908043029299840	−0.372	[−0.379 , −0.366]	2.041	[1.994 , 2.085]	82.969	[81.685 , 84.203]	4330	0.700	1.742e-05
3369088315397965056	−0.656	[−0.670 , −0.643]	1.839	[1.788 , 1.894]	40.659	[39.870 , 41.541]	6020	1.130	7.066e-05

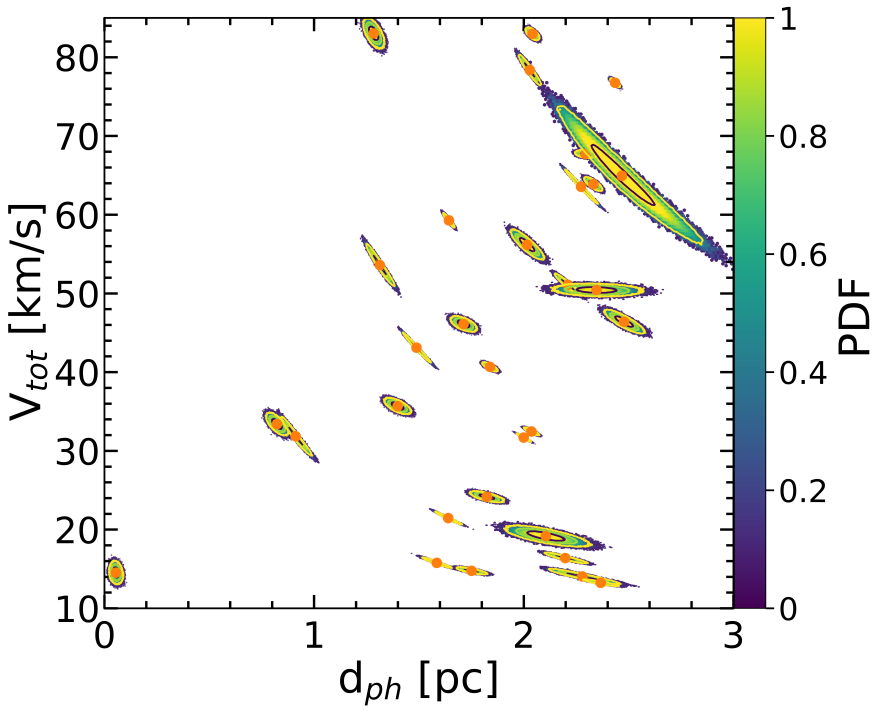

Figure 3.5: Joint probability density of the time and relative velocity of closest approach for the stars in Table 3.3.

distribution of the time and relative velocity of closest approach, showing a triangular shape with a peak toward high velocities and the present time. This is a selection effect caused by our limitation of the total studied sample to stars that are currently within 50 pc of the Sun (this means that very fast-moving stars that would approach the Sun far in the past or the future are currently not in the 50 pc volume).

We calculate the effect on a comet of a passing star that approaches to within 2.5 pc (Table 3.4), using the impulse approximation (Eq. (5.3)). We find that the change in the velocity of a comet is relatively small (in the order of 10^{-3}–10^{-4} km s^{-1}, Table 3.4). The exception is for the passage of GJ 710, which causes a velocity change of ~ 0.13 km s^{-1}, creating an important perturbation in the inner Oort cloud. Overall if only individual encounters are considered the Oort cloud comets barely feel the effect of

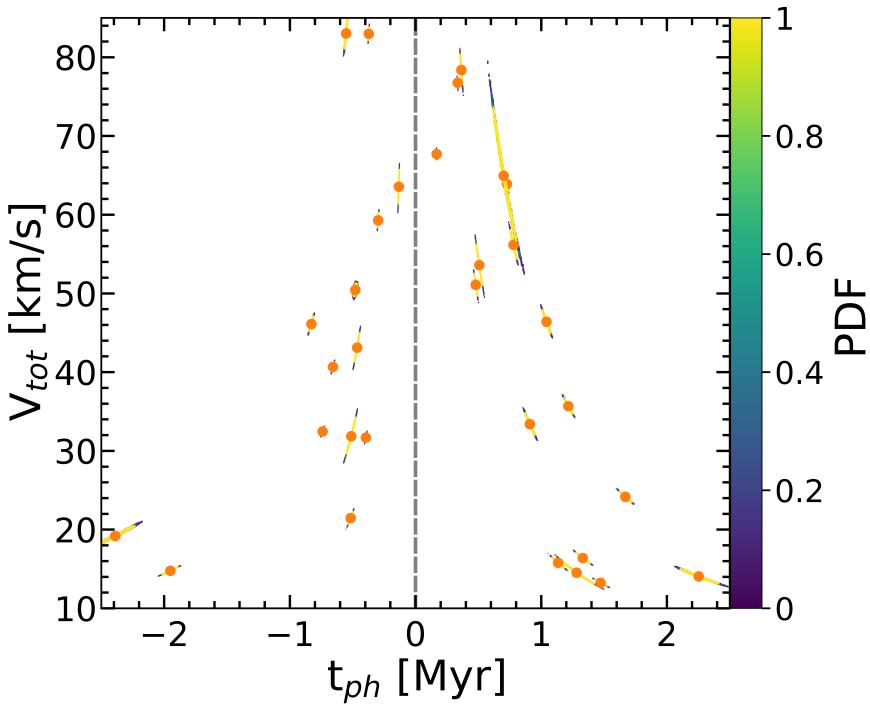

Figure 3.6: Joint probability density of the distance and relative velocity of closest approach for the stars in Table 3.3.

passing stars. The impulse approximation is based on a number of simplifying assumptions, but this approach gives us a general panorama of the individual effect of the nearby stars on a comet in the Oort cloud. In order to quantify the global effect of passing stars, it is necessary to integrate their orbits backwards and forward in time (see Sect. 3.3.1). Such a scenario is shown in the third row of Figure 3.9. The cumulative effect of nearby stars is strong enough to lift the perihelion of $\sim 0.38\%$ of the objects in the Oort cloud (Fig. 3.9, third row). Particularly the effect of GJ 710 is strong (Fig. 3.8), but encounters within $\sim$1 pc also have an important contribution.

3.3.3 The case of GJ 710/HIP 89825

For decades GJ 710 has been pointed out as the major future perturber of the Oort cloud. The first calculations using Hipparcos catalogue led to an encounter distance of 0.33 pc, 1.38 Myr from the present time (see e.g. García-Sánchez et al. 2001; Torres et al. 2018). Using *Gaia* DR1, Torres et al. (2018) pointed out that the encounter distance is even smaller, at 0.062 pc, 1.35 Myr from today (see also Berski & Dybczyński 2016; Bobylev & Bajkova 2017; Bailer-Jones 2018). With the data from *Gaia* DR2 in hand, the distance and time of closest approach have again slightly decreased to 0.054 pc and 1.28 Myr (Table 3.3,Table 3.5). de la Fuente Marcos & de la Fuente Marcos (2018) and Bailer-Jones et al. (2018) found similar but slightly discrepant results. The small discrepancy in the various results is mainly due to the orbit integration method and the Galactic potential used in their calculations, considering that the input data are the same.

A comparison of the results obtained for GJ 710 from Hipparcos, *Gaia* DR1, and *Gaia* DR2 data is shown in Fig. 3.7. Calculations were performed following the method described in Sect.3.3.1, using the astrometric data described in Table 3.5. The discrepancy between Hipparcos and *Gaia* is due to the difference in the value of the astrometric parameters and radial velocity. This results in a shift in the perihelion distance of GJ 710. Using different parameters for the Galactic potential will also lead to slightly different values (see e.g. Bailer-Jones et al. 2018). We note that the time of perihelion is more uncertain for the *Gaia* DR2 data, which is caused by the larger uncertainty in the radial velocity. Following the method described in Sect.3.3.2 and Sect.5.4, we investigated the effect of GJ 710 on a simulated Oort cloud (Fig. 3.9, first row). The perturbation because of GJ 710 lifts the semi-major axis of the comets within the region between $\sim$ 10 000 and 100 000 au (Fig. 3.8), creating $\sim$ 0.01% hyperbolic objects, while $\sim$ 0.30% of the comets gain a semi-major axis beyond the edge of the Oort cloud ($a > 100\,000$ au).

Table 3.5: Comparison of the different astrometric parameters and radial velocities obtained for GJ 710 from Hipparcos, Gaia DR1, and Gaia DR2 data. The last two rows represents the time and the closest approach distance to the Sun of GJ 710 with its respective confidence interval.

Parameters	Hipparcos	Gaia DR1	Gaia DR2
ϖ [mas]	51.12±1.63	52.35±0.27	52.51±0.04
$\mu_{\alpha*}$ [mas/yr]	1.15±1.66	-0.47±0.13	-0.45±0.08
μ_{δ} [mas/yr]	1.99±1.22	-0.18±0.09	-0.02±0.07
μ_{tot} [mas/yr]	2.30±2.06	0.50±0.16	0.46±0.11
v_{rad} [km/s]	-13.80±0.30*	-13.80±0.30*	-14.52±0.43**
t_{ph} [Myr]	1.385 [1.109,1.500]	1.353 [1.219, 1.541]	1.281 [1.109, 1.500]
d_{ph} [pc]	0.302 [0.302,0.324]	0.062 [0.014 , 0.116]	0.054 [0.003, 0.106]

*Pulkovo catalogue (Gontcharov 2006), **_Gaia_ DR2 radial velocity catalogue (Soubiran et al. 2018).

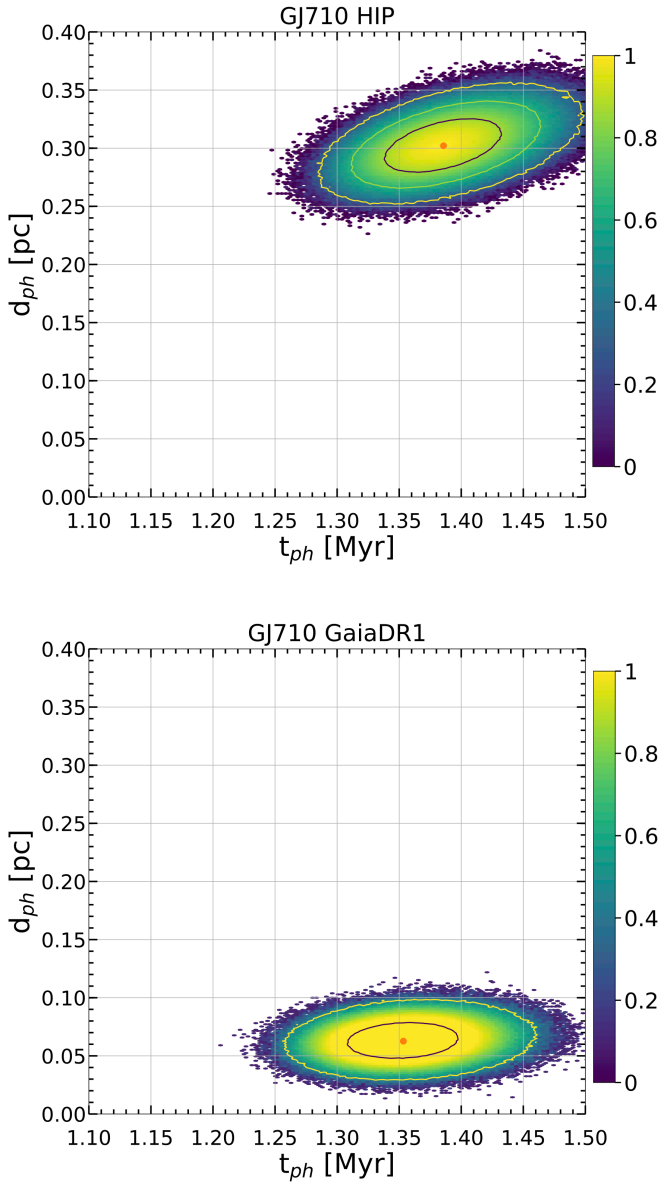

Figure 3.7: Continue...

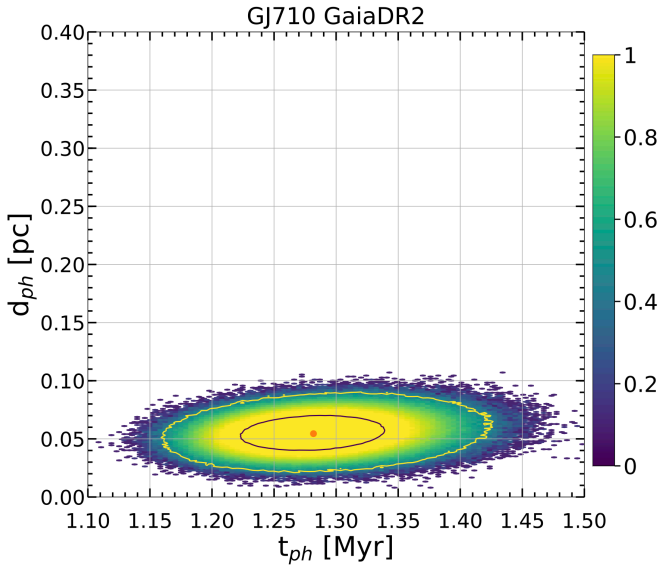

Figure 3.7: Joint distribution of the time and distance of closest approach for GJ 710. The first panel shows results obtained with Hipparcos data, while the middle and bottom panels show the results for Gaia DR1 and Gaia DR2, respectively (see Table 3.5). The contour levels indicate regions enclosing 0.60, 0.90, and 0.99% cumulative probability (color bar).

Section 3.4

Dynamical evolution of the Oort cloud

As pointed out by Heisler & Tremaine (1986) the Galactic tidal field is a major contributor to Oort cloud perturbations at large distances, while as we showed in Sect. 3.3.2 the cumulative effect of passing stars can also lead to substantial perturbations of the Oort cloud comets. In this section we study the cumulative effects of the known stellar encounters (Table 3.4) and the Galactic tidal field over the interval of 20 Myr centred on the present time. This provides a lower limit to the combined effect of stellar encounters and the Galactic tidal field on the dynamical evolution of the Oort cloud.

3.4.1 Numerical model

We use the Astrophysical Multi-purpose Software Environment – AMUSE (Portegies Zwart et al. 2009; Pelupessy et al. 2013; Portegies Zwart et al.

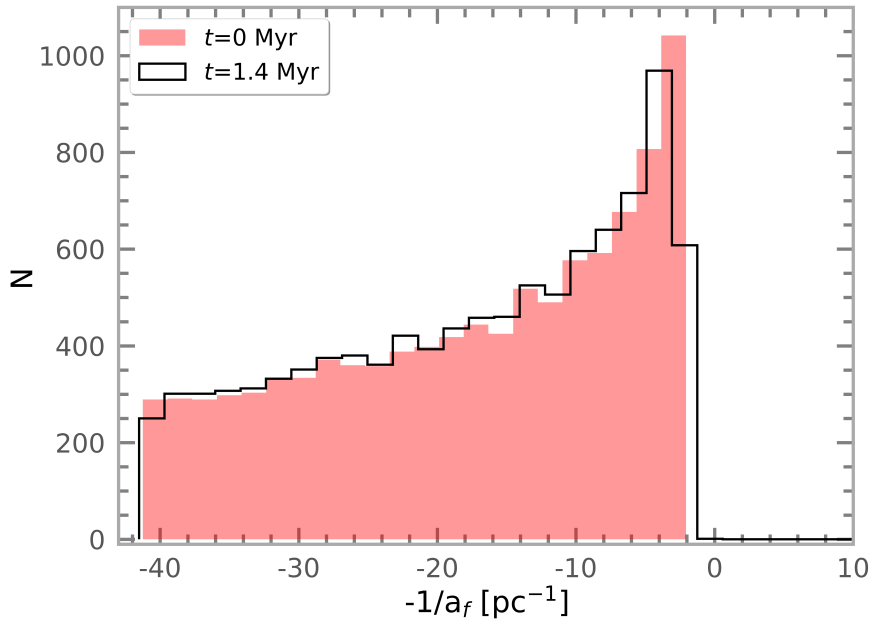

Figure 3.8: Histogram of the orbital energy distribution of the particles in the Oort cloud, before and after the encounter with the star GJ710. The red histogram corresponds to the initial semi-major axis distribution, and the black curve to the final one.

2013b; Portegies Zwart & McMillan 2018) – for our calculations. Following the works of Rickman et al. (2008) and Hanse et al. (2016) we first construct an isotropic Oort cloud of $10,000$ test particles (Fig. 3.9, first row). The distribution of Oort cloud particles is spherically symmetric and isotropic, and they follow a uniform distribution in the orbital elements $\cos i$, ω, Ω, and M. The initial eccentricities, e, are selected with a probability density distribution $p(e) \propto e$ and the perihelia, q, are chosen outside of the planetary region ($q > 32$ au). The semi-major axes, a, are distributed proportional to $a^{-1.5}$ over the range 3×10^3–10^5 au. In order to ensure a thermalised Oort cloud (e.g. Duncan et al. (1987); Dybczyński (2002); Rickman et al. (2008)) we used a radial density profile of $r^{-3.5}$ (where r is the distance between the comets and the Sun).

Subsequently we used the GPU-accelerated direct N-body code ABIE (Cai et al. in preparation) with a fifteenth-order Gauss-Radau integrator

(Everhart 1985) optimised for close encounters. We couple ABIE and the Gala package in such a way that ABIE advances the positions of the Oort cloud particles and Gala calculates the accelerations on each particle due to the Galactic tidal field, based on the positions provided by ABIE. The calculated accelerations are subsequently inserted into the Gauss-Radau integrator in ABIE as additional forces. Using the catalogue of nearby stars (Table 3.3), we selected all the stars (31) that are predicted to pass within 2.5 pc of the Sun (Table 3.4) ± 10 Myr from today. These stars are included in the integrator with their present-day positions and velocities with respect to the Sun. Hence we evolve a system for a period of 20 Myr which consists of one host star (the Sun) surrounded by $10,000$ test particles (Oort cloud) under the influence of external perturbations due to passing stars and the Galactic tidal field.

3.4.2 Galactic tide and Gaia star perturbation

In order to disentangle the effects of the Galactic tidal field and the encounters with stars identified in *Gaia* DR2 we considered three main cases for external perturbations, *Galactic tidal field, Gaia stars, Galactic tidal field + Gaia stars*. We focus now on the effect of the external perturbations considering an extended Oort cloud ($a \leqslant 100\,000$ au). The first row of Fig. 3.9 shows the initial conditions followed by the final perihelion distance as a function of the final semi-major axis for the three scenarios previously discussed. Considering a short integration of 20 Myr (10 Myr in the past, and 10 Myr in the future). The green area represents the original location of the ejected particles (yellow dots).

The effect of the Galactic tidal field on the Oort cloud decreases from the outskirts to the inner regions of the cloud (second row Fig. 3.9). The particles at the edge of the cloud suffer a considerable change in their orbital elements. Specifically, for $\sim 0.91\%$ (yellow dots, Fig. 3.9) of the objects, their semi-major axes increase up to interstellar distance ($a > 100\,000$ au). The particles in the inner Oort cloud remain unaffected. A small fraction of the particles ($\sim 0.02\%$) acquire hyperbolic orbits. When *Gaia* stars are the only perturber (Fig. 3.9, third row) their effect is much less pronounced than that of the Galactic tidal field in particular in the outskirts on the Oort cloud. The effect of *Gaia* stars is dominated by the star GJ 710 (Fig. 3.8). However, the cumulative effect of relatively distant encounters ($\sim$ 1pc) helps to change the semi-major axis of $\sim 0.38\%$ of the comets in the

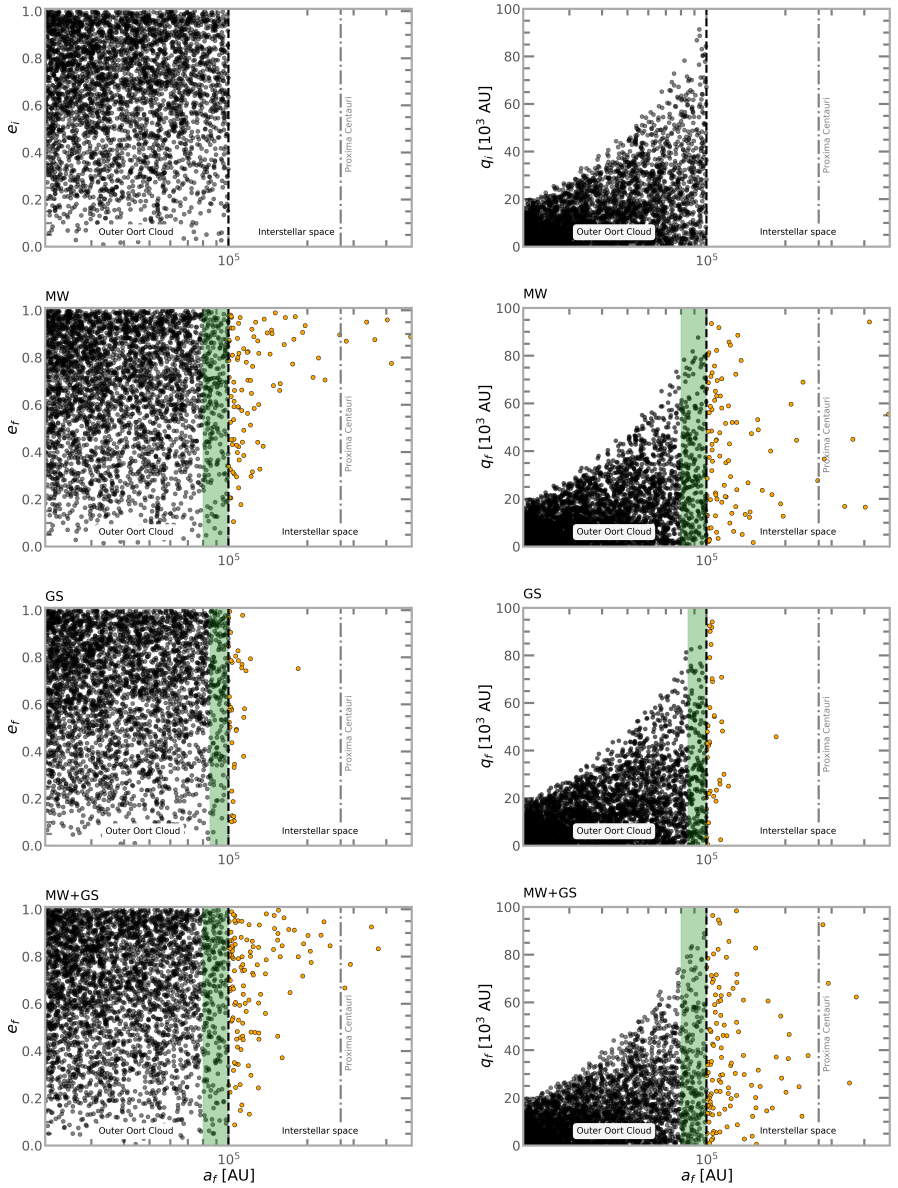

Figure 3.9: Final eccentricity and perihelion as a function of final semi-major-axis, for a total integration of 20 Myr. The first row corresponds to the initial conditions. The second and third rows show the effect of the Galactic tidal field and Gaia stars, respectively. The last row corresponds to the combined effects of the Galactic tides and Gaia stars. The green area corresponds to the initial position of the ejected particles, coloured yellow.

outer Oort cloud, whereas 0.01% of the outer Oort cloud objects acquire hyperbolic orbits.

The combination of the Galactic tidal field and *Gaia* stars (Fig. 3.9, last row) enhances the perturbations on the Oort cloud, causing 0.03% of the initial objects to become unbound from the solar system, while $\sim 1.12\%$ acquire orbits with semi-major axis in the interstellar regions, i.e., $a \geqslant 100\,000$ au. In all three scenarios for external perturbations, a considerable population of objects with $a \geqslant 100\,000$ au is created. Their orbits remain elliptic, but the effect of external perturbations lifts their semi-major axis beyond the Oort cloud (yellow dots, Fig. 3.9). This effect is only relevant for the outermost regions of the Oort cloud ($\sim 80\,000$–$100\,000$ au). The orbital elements of the particles in the inner parts of the cloud will not be affected as strongly.

We now consider a compact Oort cloud with semi-major axes up to $50\,000$ au. The effect of the Galactic tidal field has a negligible effect (first panel, Fig. 3.10) over the particles in the cloud. The second panel in Fig. 3.10 shows the effect of the Gaia stars. The effect of GJ 710 is prominent, and causes a major perturbation. The last panel in Fig. 3.10 shows that the effect of the *Gaia* stars dominates over the Galactic tidal field, however it is the combined effect which efficiently increases the number of particles (by $\sim 1.20\%$) with semi-major axis beyond the limits of the cloud ($a > 50\,000$ au).

We conclude that the cumulative effect of passing stars and the Galactic tidal field are efficient mechanisms in the creation of comets for which the semi-major axis is larger than the extent of the Oort cloud ($a > 100\,000$ au), but with bound and eccentric orbits. Hereafter we refer to such objects as transitional interstellar comets (TICs). If we consider an Oort cloud with $a \leqslant 100\,000$ au, the Galactic tidal field is the major perturber, while for an Oort cloud with $a \leqslant 50\,000$ au passing stars provide the major effect, mainly due to the close encounter with GJ 710 (Fig. 3.8).

For long timescales (on the order of gigayears), the synergy between Galactic tides and stellar encounters to bring comets into the observable zone is now well understood (Rickman et al. 2008; Fouchard et al. 2011). Both perturbations strongly depend on the semi-major axis of the comets. In general the Galactic tidal field rapidly changes the perihelia of the outer regions, while passing stars are a good mechanism to eject or inject particles when a close encounter happened (see e.g, Portegies Zwart & Jílková 2015). For short timescales (~ 20 Myr), the Galactic tide and stellar en-

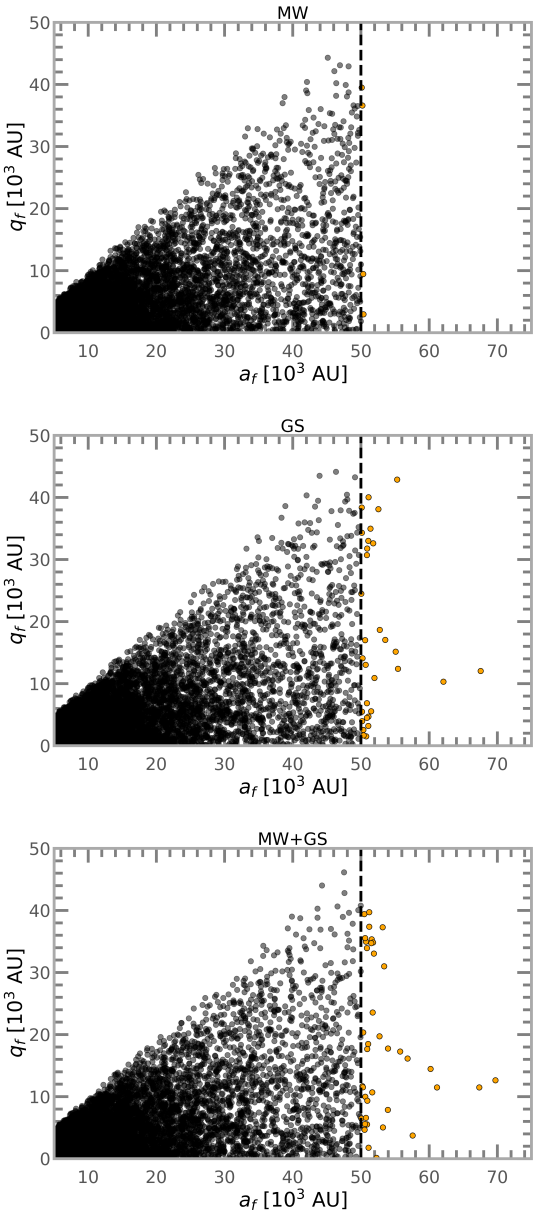

Figure 3.10: Final perihelion as a function of final semi-major axis for an Oort cloud size of 50,000 au. The first panel shows the effect of the Galactic tidal field (marked as a MW). The second and third panels show the effect of Gaia stars (GS) and the combination of both the Galactic tide and Gaia stars (MW+GS), respectively. Black dots represent the particles in the Oort cloud, while the yellow dots represent the ejected ones.

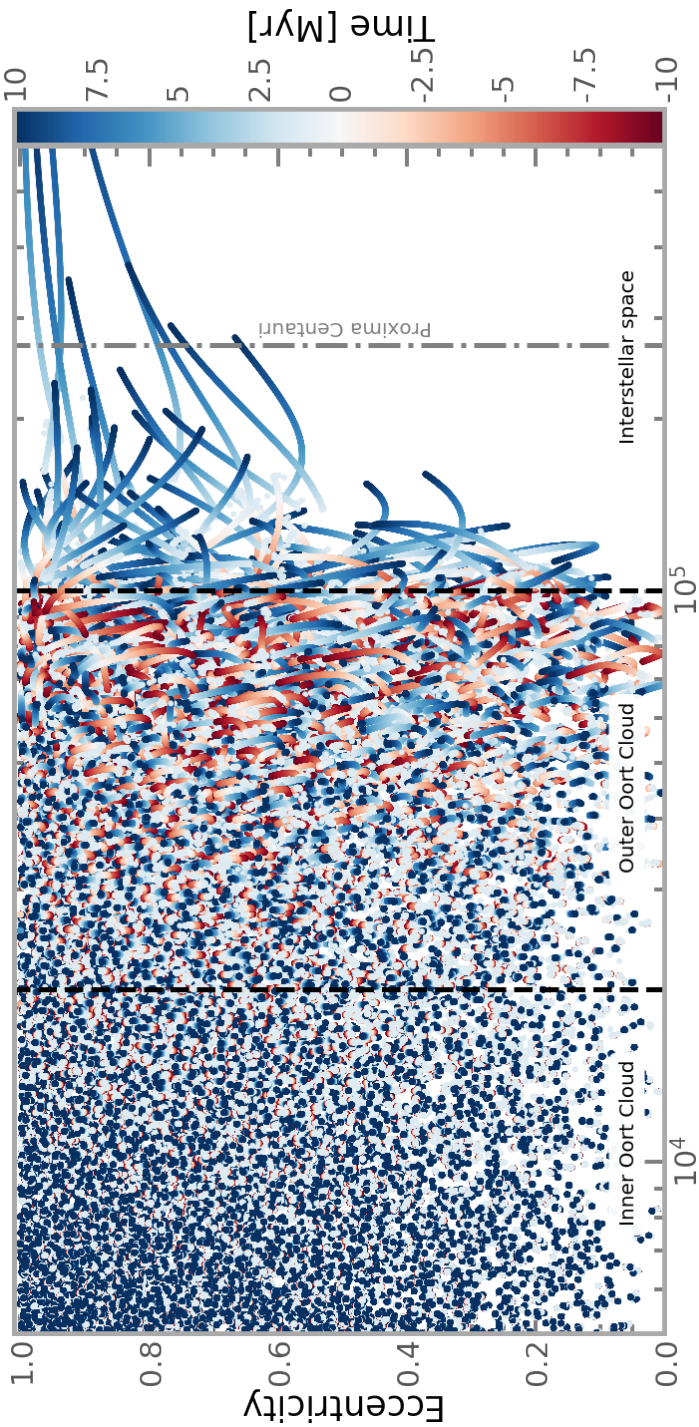

Figure 3.11: Orbital evolution of the particles in the simulated Oort cloud. The figure shows the evolution of the eccentricity as a function of the semi-major axis over the period of 20 Myr (±10 Myrs.). The colour bar represents the integration time. An animation can be found at: https://home.strw.leidenuniv.nl/~storres/#Research

.

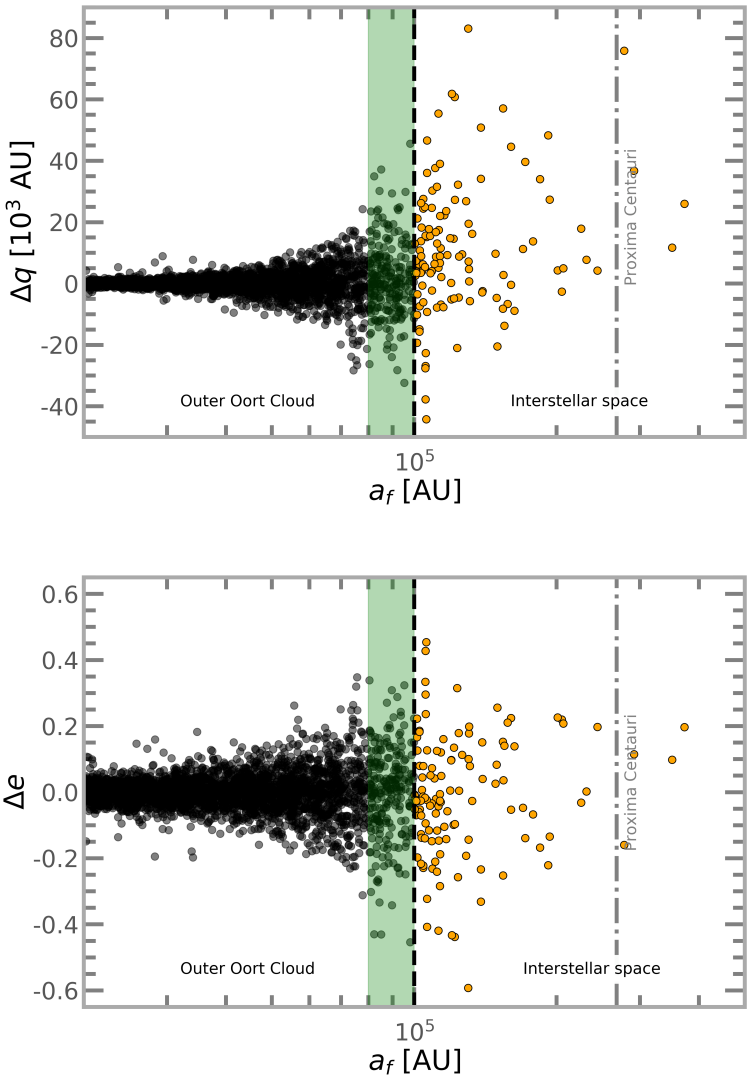

Figure 3.12: Mean perihelion and eccentricity changes as a function of the semi-major axis of the comets. The green area corresponds to the region of the initial position of the particles ejected, represented as a yellow dots.

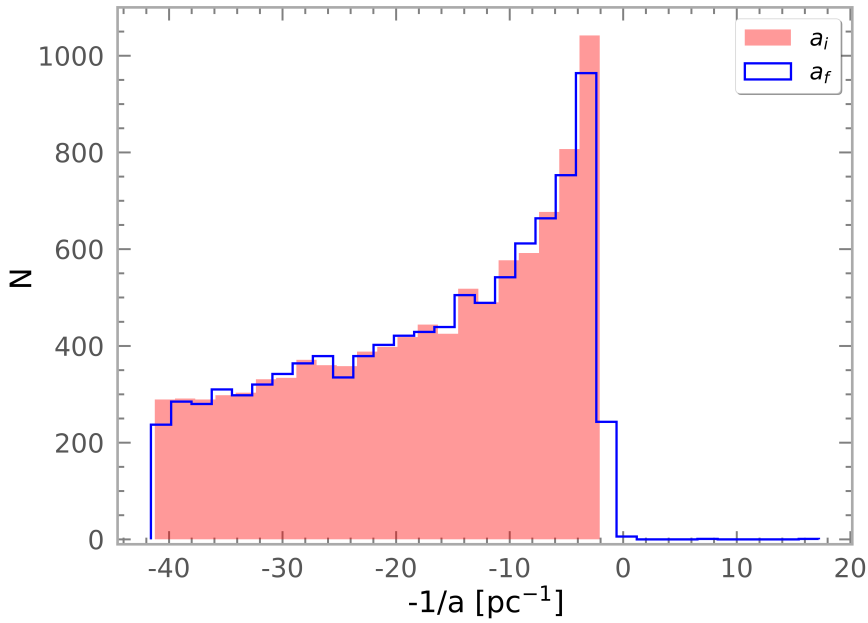

Figure 3.13: Histogram of the orbital energy distribution of the particles in the Oort cloud. The blue curve corresponds to the final semi-major axis, while the red curve shows the initial distribution.

counters prove to be an efficient mechanism for the creation of TICs. The outermost part of the cloud ($\sim 80\,000$–$100\,000$ au, Fig. 3.11) is heavily perturbed, whereas the innermost part remains unchanged (3000–$50\,000$ au, Fig. 3.11). This implies that the edge of the Oort cloud is sensitive to external perturbations and is relatively easy to strip. The particles in the outermost part of the Oort cloud have a considerable change in their orbital elements. The change of the perihelion and eccentricity increases as a function of the semi-major axes (Fig. 3.12), whereas the semi-major axes reach interstellar distances. These objects previously referred to as transitional interstellar comets remain bound to the Sun with eccentric orbits (Fig. 3.13). The detailed effects of subsequent perturbations due to passing stars and the Galactic tidal filed will determine if these objects will return to the solar system or become unbound.

Considering the efficiency of external perturbations on circumstellar comet clouds in the creation of interstellar objects, and noting that Valtonen & Innanen (1982) pointed out that objects with a relative velocity above 0.5 km/s can probably enter and leave the solar system, we speculate that a 'cloud' of objects exists in interstellar space which overlaps with our Oort cloud and constantly exchanges material with it. An indication that this may be the case was provided by the first interstellar comet detected, 'Oumuamua (Williams 2017), which opened a new era in the study of interstellar objects. Estimates of the local density of interstellar objects range from 10^{14} pc^{-3} (Portegies Zwart et al. 2018), to 8×10^{14} pc^{-3} (Jewitt et al. 2017), to 2×10^{15} pc^{-3} (Do et al. 2018). The existence of an interstellar comet cloud could partly explain the slightly hyperbolic comets and potential interstellar objects that might have been detected in the solar system but not yet classified as such (see e.g. de la Fuente Marcos & de la Fuente Marcos 2019). A future detailed study of the evolution of the TICs created by the tides and stellar encounters is needed to draw more solid conclusions.

The results presented here are based on the assumption of a hypothetical present day spheroidal cloud of comets extending up to $100,000$ au from the Sun. If we consider a smaller structure (Fig. 3.10), passing stars are the main perturbers, while the Galactic tidal field barely influences the orbit of the comets. In addition we stress that our sample of stars considered as perturbers of the Oort cloud is incomplete due to the *Gaia* survey limits combined with our data quality filtering and the upper limit we imposed on the distance to the stars in our sample. A more complete inventory of Oort cloud perturbers would increase the effects of the stellar encounters.

Section 3.5

Summary and Conclusions

In this work we present a study of the combined effect of the Galactic tidal field and close stellar encounters predicted to occur over a time interval of 20 Myr around the present on the Oort cloud of the solar system. Our focus is on the loss of comets to interstellar space. Following Rickman et al. (2008), we first presented a simple model of stellar encounters based on data compiled for 13 spectral types of the stars in the solar neighbourhood. We confirm that individual perturbations of randomly passing stars cannot alter the orbits of the comets in the Oort cloud unless a very close encounter

occurs. However, from a consideration of the stellar encounter statistics we show that the comets in the cloud may be lost to interstellar space over a short period of time due to the cumulative effect of stellar encounters.

Motivated by this result we used *Gaia* DR2 data to identify $14,659$ stars passing within 50 pc of the Sun over the time period of ± 10 Myr centred on the present. Out of this sample 31 stars are predicted to be major perturbers of the Oort cloud, approaching the Sun to within 2.5 pc. This catalogue of perturbing stars (presented in Table 3.3) constitutes an astrometrically clean sample, which is nevertheless incomplete due to the *Gaia* survey limitations, the upper limit imposed on the distance to the stars in the sample (50 pc), and the strict data-quality filtering. Our estimates of the effect of known stellar encounters is therefore conservative (we note that Bailer-Jones et al. 2018, find a larger number of stellar encounters from *Gaia* DR2 due to their less stringent data-quality filtering). Using the impulse approximation (Eq. (3.1)) we then calculated the impulse that each star passing within 2.5 pc of the Sun imparts to a comet in the Oort cloud. We found that (as expected) the effect of individual encounters is relatively small (on the order of 10^{-3} to 10^{-4} km s^{-1}). The cumulative effect of *Gaia* stars was then investigated. We found that the collective effect of stars passing within $\sim$ 1pc can lift the perihelion of members of the Oort cloud in a relatively short period of time.

Finally, we focused our study on the combined effect of multiple stellar encounters and the Galactic tidal field on a simulated Oort cloud. To achieve this we used a detailed N-body simulations, evolving a system of one host star (the Sun) surrounded by 10,000 test particles (the Oort cloud) and affected by three different sets of external perturbations (*Gaia* stars only, Galactic tidal field only, and the combination of both), over a period of 20 Myr (± 10 Myr centred on today). When we consider an extended Oort cloud ($a \leqslant 100\,000$ au), we find that the effect of the Galactic tidal field alone leads to the creation of TICs of around 0.91% of the initial comets, while the collective effect of the passing stars only leads to a smaller fraction of 0.38%. For the compact model of the Oort cloud ($a \leqslant 50\,000$ au), passing stars dominate the perturbations, mainly due to the star GJ 710, while the effect of the Galactic tidal field is almost negligible. Overall for an extended cloud, the Galactic tide dominates over the passing stars, for the case of a compact cloud the opposite is true. However, it is the combined effect of passing stars and the Galactic tidal field which significantly increases the perturbation on the Oort cloud. These combined effects raise the semi-major axis of around 1.12% of the initial particles for the compact

model, and $\sim 1.20\%$ for the extended one, up to the interstellar regions (i.e. a > 100 000 au). The estimates presented in this work are conservative and based on a small sample of known stars that pass near to the Sun during ± 10 Myr. The effects of a more complete sample will increase the number of TICs. Overall the external perturbations are an efficient mechanisms in the formation of interstellar comets over a short period of time (in the order of tens of megayears).

The further evolution of the transitional interstellar comets depends on the perturbations introduced by passing stars and the Galactic tidal field. These perturbations determine whether the transitional interstellar comets will remain bound to the solar system or eventually become interstellar comets. Under the hypothesis that other planetary systems also possess Oort cloud-like structures, they most probably experience the same mechanism of erosion due to external perturbations. This leads us to speculate that there is a large population of cometary bodies that occupy interstellar space. Therefore, visits to the solar system by interstellar comets such as 'Oumuamua may well be a frequent occurrence.

Acknowledgements We thank the referee for the constructive reports and helpful suggestions to improve the present work. ST expresses his gratitude to the Mexican National Council for Science and Technology (CONACYT) for the grant #291004-410780; to Leiden Observatory for the unconditional support; and to Daniel Hestroffer, Eric Mamajek, Konstantin Batygin, and Ylva Götberg, for the discussions and comments on the manuscript. This project was shaped in part at the 2018 New York Gaia Sprint. This work was supported by the Netherlands Research School for Astronomy (NOVA) and by NWO (grant #621.016.701 [LGM-II]). This work has made use of data from the European Space Agency (ESA) mission *Gaia* (https://www.cosmos.esa.int/gaia), processed by the *Gaia* Data Processing and Analysis Consortium (DPAC, https://www.cosmos.esa.int/web/gaia/dpac/consortium). Funding for the DPAC has been provided by national institutions, in particular the institutions participating in the *Gaia* Multilateral Agreement. This work was carried out on the Dutch national e-infrastructure with the use of *Cartesius* the Dutch national supercomputer and the support of SURF Cooperative.